

Improved Performance of Secondary Doped PANI and Its Application in Coated Zn//PANI Composite Film as Electrodes with Controllable Thickness for Rechargeable Batteries

Huijun Cao^{1,2*}, Xiangbin Xu¹, Shihui Si², Jirui Li¹ and Degeng Li²

¹Department of Pharmaceutical and bioengineering, Hunan Chemical Vocational Technology College, Zhuzhou 412004, PR China

²College of Chemistry and Chemical Engineering, Central South University, Changsha 410083, PR China

Keywords: Zinc composite anode, Secondary doped polyaniline composites cathode, Electrodes preparation by coating, Highly stable rechargeable battery

Abstract: To improve the conductivity of pure polyaniline (PANI), compact scale-like PANI secondary doped with lithium chloride (LPANI) was prepared after the in situ synthesis of PANI powder using the constant current method and 4,4'-diaminobiphenyl (DABP) as an additive in hydrochloric acid (HCl). The dense morphology of obtained LPANI was found to promote the charge transfer in the PANI chains and intermolecularly. The oxidation peak currents of LPANI with DABP additive were nearly three times higher than those of the LPANI and much higher than those of in situ doped PANI with HCl without additive. The application of LPANI in composite film batteries was also examined. Both the LiCl-PANI/TiO₂/C/DABP composite (LPTCD) cathode and Zn/ZnO/MgO/CMC-Na composite (ZZMCN) anode were prepared by evenly coating at controlled thicknesses of 0.20 mm and 0.04 mm, respectively. A coated Zn composite/coated LPANI composite battery was designed, with an open voltage of approximately 1.5 V in ZnCl₂+LiCl electrolyte solution. The battery charge/discharge cycle performance was determined between 0.7 V and 1.7 V. The discharge capacity of the cathode reached 131.4 mAh·g⁻¹ at a current density of 2 mA·cm⁻². During 35 charge/discharge cycles, the average decrease in the discharge capacity of each cycle was 0.07%, indicating that the cycle performance and stability of the battery could contribute to applications that replace traditional lead-acid batteries.

1 INTRODUCTION

The application of polyaniline (PANI) in the fields of super capacitor and rechargeable batteries has become a hot research topic due to the high conductivity, excellent redox reversibility, environmental friendliness and low cost of materials (Skotheim et al., 1997; Ghanbari et al., 2006; Liu et al., 2006; El-Nowihy et al., 2017; Wang, 2018). Traditional nickel-cadmium batteries (Nishio and Furukawa, 2007; Gao et al., 2016; Pourabdollah and Kobra, 2017; Yazvinskaya et al., 2017) and lead-acid batteries (Wills et al., 2010; Collins et al., 2010; Pletcher et al., 2008; Pletcher et al., 2008; Li et al., 2009; Collins et al., 2010) are being gradually withdrawn from the market because of their high pollution. Lithium batteries are currently too expensive, and the organic solvents used in the

battery cause safety issues (Liang et al., 2012; Wilken et al., 2013; Zhang et al., 2015; Hu et al., 2017; Yoshitaka et al., 2017). Thus, research on low-cost and environmentally friendly Zn//PANI rechargeable battery with water-based electrolyte has attracted the attention of the scientific community (Dinh et al., 1998; Kan et al., 2002; Vatsalarani et al., 2005; Pozo- Gonzalo, 2015).

However, in depth research on Zn//PANI has shown that PANI battery systems have a low active material utilization rate, decompose easily after overcharge, and self-discharge, and other problems, which directly limit the industrial applications of such batteries (Li et al., 2008; Sivaraman et al., 2008; Liu et al., 2018). There are two main reasons for this problem. First, the anions de-dope during the discharge process of PANI, leading to the gradual transformation of the conductive PANI to a semiconductor or an insulator, which increases the

internal resistance of the battery, resulting in PANI being ineffective. Second, PANI is trapped, causing diffusion problems. During the charge/discharge process, the anions can not diffuse internally into macro-molecular PANI, which causes a charge imbalance in the internal PANI structure, resulting in electrode polarization and low conductivity (Mirmohseni and Solhjo, 2003; Bogdanovic et al., 2014).

Researchers have proposed many solutions to solve the low electrical conductivity problem (El-Nowihy et al., 2017; Wang et al., 2018; García-Lugo et al., 2018). The most commonly used method is adding a conductive reagent, such as graphite, to the PANI particles to reduce the internal resistance of the Zn//PANI battery (Arjomandi and Tadayyonfar, 2013; Zhao et al., 2018; Arafa et al., 2013; Hui et al., 2017; Yi et al., 2017; Hun et al., 2018; Liu et al., 2014; Liu et al., 2017). The disadvantages of low solubility in water and common organic solvents keeps PANI particles from easily forming a film. High pressure is usually used to ensure the combination of graphite and PANI, but this method also leads to the penetration of the electrolyte and ion diffusion problems. Electrochemical polymerization has been used to prepare an evenly dispersed PANI film on conductive current collector materials, such as gold, platinum, or graphite. The thickness of the electro-polymerized PANI film is usually limited to only a few dozen microns. Thus, the mass of the current collector is much larger than the load of the electroactive material, which causes the integral energy density of the battery to dramatically decrease, making industrial applications difficult. Although the coating method has been frequently applied to lithium batteries (Paral et al., 2018; Rana et al., 2014; Tran et al., 2015; Pirkarami et al., 2013; Ramirez et al., 2017; Zhang et al., 2018), the polyvinylidene fluoride binder used in lithium batteries is not suitable for the PANI film electrode system, because active PANI film electrode materials prepared with polyvinylidene fluoride binder are easily stripped from the substrate.

In this study, a dense PANI was prepared by electrochemical polymerization, at constant current using DABP as an additive to the HCl solution, to realize the first doping, followed by the secondary doping of PANI with a pseudo proton acid of lithium ions (Li^+). The morphology, structure and electrochemical performance of LPANI were observed. The application LPANI in composite film batteries was also examined. Both the LPTCD cathode and ZZMCN composite anode were

prepared by evenly coating at controlled thicknesses of 0.20 mm and 0.04 mm, respectively. Graphite was used as the cathode current collector due to its low cost and good conductivity. The charge and discharge properties of the battery were studied, which revealed an application potential of the proposed batteries.

2 EXPERIMENTAL SECTION

2.1 Preparation of Graphite Paper and Oxidation Pretreatment

An expandable graphite suspension was mixed with hydroiodic acid at a volume ratio of 15:1 and uniformly coated on a polyethylene film, which strengthened of a current collection to a certain degree. The mixture was dried at 60°C for 6 h in a vacuum oven, cooled, rinsed successively with ethanol and twice with distilled water, and put into a vacuum oven at 40°C for 8 h to prepare the sparingly porous product. The dried graphite paper was used as the electrode current collector. Prior to the experiments, the graphite paper was soaked in a concentrated nitric acid solution for surface oxidation treatment, washed with ethanol, rinsed twice with distilled water, and dried in an oven. The treated graphite paper, which had a thickness of approximately 0.050 mm, was cut into 1×2 cm bars.

2.2 Preparation of Secondary Doped PANI with Lithium Ions

Two kinds of singly doped PANI powder were prepared by electrochemical polymerization by in situ doping with HCl: one contained with the DABP additive, and the other did not contain the additive. The in situ doped PANI powder was synthesized galvanostatically on a graphite plate at a current density range of 3–5 $\text{mA}\cdot\text{cm}^{-2}$ for 24 h in a solution consisting of 0.5 M aniline and 1.0 M HCl with or without 25 mM DABP as additive, and oxygen was excluded by bubbling nitrogen into the electrolyte without stirring. Before the polymerization experiments, the graphite electrode surface was mechanically polished successively with 600, 800, 1200 grade emery papers and cleaned in an ultrasonic bath in a mixture of water and ethanol. After polymerization, PANI was collected on the graphite plate by scratching with a plastic knife, and then rinsed with dilute HCl solution and deionized

water until the filtrate appeared colorless, followed by drying in a vacuum oven. The resulting dark green powder was singly doped PANI. The in situ doped PANI was added to 0.1 M ammonia solution to remove the HCl, stirred at room temperature for 6 h, filtered, and rinsed to obtain the emeraldine base form of PANI (EB). The EB was soaked in different concentrations (0.3 M, 0.5 M, 0.7 M) of LiCl or 0.3 M CH_3COOLi , stirred at 10–35°C for 2–10 h, and then filtered and dried, resulting in secondary doped PANI (coded as LiCl-PANI (LPANI), CH_3COOLi -PANI (APANI), respectively). The secondary doped PANI powder was subjected to grinding with a cutting mill to yield micro-sized PANI particles. The PANI powder was dried in a vacuum oven at 80°C for 24 h.

The third kind of in situ doped PANI powder was chemically polymerized as follows: 0.1 mol of pure aniline was dissolved in 400 mL of a 1 M HCl solution. Then, 0.1 mol of $(\text{NH}_4)_2\text{S}_2\text{O}_8$ was added slowly to the solution, and the mixture was stirred at room temperature for 10 h. After the reaction was completed, the green polyaniline salt was precipitated and washed with absolute ethanol, dilute HCl solution, and deionized water until the wash was colorless. The polyaniline product was cut into microparticles according to a previous method.

2.3 Preparation of the Secondary Doped PANI Composite Cathode and Zn Composite Anode by the Coating Method

The secondary doped PANI composite cathode was fabricated using the coating method. A certain amount of the prepared secondary doped PANI powder was evenly ground, and the graphite and TiO_2 powders were added and mixed. Then, DABP, as the binder, was added dropwise into the mixture. The final mixture was stirred into a paste, and coated on one side of the prepared graphite paper. The other side was sealed with insulating glue and dried in a vacuum oven at 90°C for 2 h to produce the PANI composite cathode.

The Zn composite anode was also prepared by using the coating method. A paste containing 92 wt% Zn powder, 4 wt% ZnO powder, 2 wt% MgO powder, 1 wt% sodium carboxymethyl cellulose, 1wt% surface active, and a small amount of binder was evenly mixed and coated on copper foil. The coating thickness was approximately 0.04 mm. The Zn composite anode was dried in a vacuum oven and pressed flat by a tableting machine.

2.4 Characterization Methods

The LPANI was compressed with KBr for Fourier transform infrared (FT-IR) spectroscopy detection over a wave number range of 400–4,000 cm^{-1} . The morphology of the LPANI was investigated by scanning electron microscopy (SEM) at an acceleration voltage of 20 kV ($\times 10,000$). The cyclic voltammogram (CV) of LPANI was observed with a three-electrode system over the scanning potential range of -0.2–0.8 V at a scanning rate of 50 $\text{mV}\cdot\text{S}^{-1}$ from negative to positive scanning position, then in reverse. The conductivity was measured by a FT-341 four-probe conductivity testing system. All electrochemical testing was carried out with CHI660D electrochemical analyzer (Chen Hua Instrument Co., Shanghai, China) using a three-electrode system that consisted of a saturated calomel electrode (SCE) as the reference electrode, a platinum wire as the counter electrode, and the LPANI power coated on graphite paper as the working electrode. All charge/discharge experiments on the Zn composite//PANI composite battery were conducted with a BTS battery test system (Neware Ltd., Shenzhen, China). All potentials refer to the SCE.

3 RESULTS AND DISCUSSION

3.1 Properties of the Secondary Doped PANI Cathode Material

The bulk densities, determined by wax covering method, were estimated to be 0.52 $\text{g}\cdot\text{cm}^{-3}$, 1.38 $\text{g}\cdot\text{cm}^{-3}$, 1.13 $\text{g}\cdot\text{cm}^{-3}$ for the three kinds of LPANI powders which were prepared by chemical polymerization, secondary doping with LiCl after in situ doping by electrochemical polymerization, and only in situ doping electrochemical polymerization, respectively. The LPANI powder prepared by electrochemical polymerization with the additive appeared to have an overwhelmingly higher bulk density than the chemically synthesized powder, because of the chain extension and crosslinking effect of the binder function of DABP and the secondary doping with LiCl. Figure 1 shows the SEM images of these kinds of PANI powder. The compact scale-like micro-structure of the electrochemical polymerized LPANI with additive (Figure 1a), the sponge-like structure of the singly in situ doped electrochemical polymerized PANI with additive (Figure 1b), and the granular and bulky

morphology of the chemically polymerized LPANI (Figure 1c) were observed. The scaly morphology of the electropolymerized LPANI facilitated contact between the PANI particles, due to the conjugation lengthening function of DABP (Yesappa et al., 2017; Pandey et al., 2016; Silva et al., 2014; Sevil et al., 2014; Mini et al., 2014). We speculated that, the scaly structure of the electropolymerized PANI particles would impart excellent electrochemical activity. This presumption was confirmed by testing the electrical conductivity at room temperature, which yielded values of $2.37 \text{ S}\cdot\text{cm}^{-1}$, $1.38 \text{ S}\cdot\text{cm}^{-1}$, and $0.52 \text{ S}\cdot\text{cm}^{-1}$ for the electro-polymerized LPANI with additive, singly in situ doped electro-polymerized PANI with additive, and the chemically polymerized PANI.

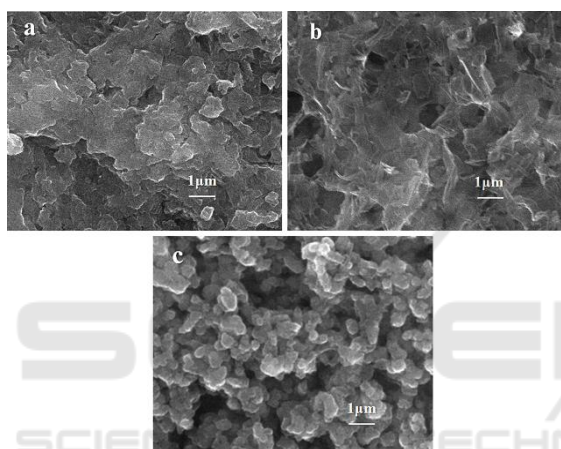


Figure 1: Scanning electron microscope images of LPANI: a, electro-polymerized LPANI with additive; b, singly in situ doped electropolymerized PANI with additive; c, the chemically polymerized PANI.

Figure 2 shows that the additive and preparation method influence the electrochemical activity of electropolymerized LPANI in 0.5 M ZnCl_2 electrolyte solution (pH 4.0). Two mutually overlapping oxidation peaks are observed between 0.30 V and 0.65 V under positive scanning, while the negative scanning process provides only a reduced peak at 0.21 V , which was distinctly different from that of the in situ doped electropolymerized PANI, owing to the presence of two types of positive doping ions (H^+ , Li^+) and only one type of negative doping ions (Cl^-) in the polymerization process. The oxidation peak current of LPANI with DABP additive (0.17 A) at 0.48 V is nearly three times higher than that of LPANI without additive (0.06 A) and much higher than that of HCl in situ doped PANI without additive, which is consistent with the previous conclusion from the

CV, suggesting that the electrochemical activity is enhanced for the preparation of LPANI with DABP additive and the secondary doping with LiCl. Chemical doping of the transition metal Zn^{2+} ions has been reported in previous studies, indicating that Zn^{2+} ions are involved in the pseudo-protonation of PANI during the chemical redox process (Xu et al., 2014; Xu et al., 2017; Taheri et al., 2018). In this case, Zn^{2+} ions also participate in the pseudo-protonation of the LPANI film during the electrochemical redox process. However, as illustrated in Figure 2(a,b), due to the large radius of Zn^{2+} , compared with that of protons, the relatively slow process for Zn^{2+} ions to become embedded in the PANI chain leads to a positive shift in the first oxidation peak of approximately 0.1 V , which shortens the distance between the two oxidation peaks and improves the redox reversibility. Therefore, LPANI allows the PANI composite cathode to operate at higher current density.

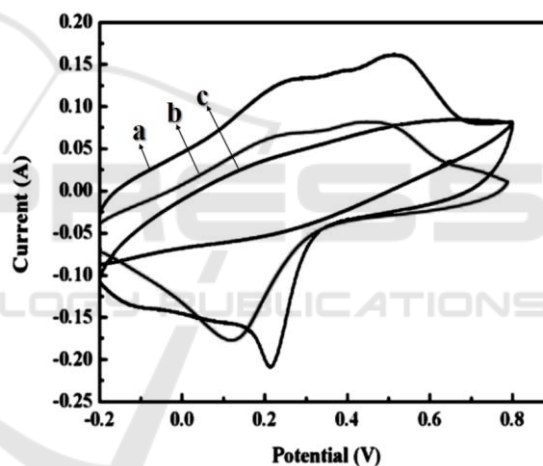


Figure 2: Cyclic voltammogram of LPANI in 0.5 M ZnCl_2 electrolyte solution (pH 4.0) before secondary doping: a, electro-polymerized LPANI with DABP additive; b, electro-polymerized LPANI without additive; c, in situ electro-polymerized PANI without additive.

3.2 Characteristic Analysis of the Secondary Doped PANI

Figure 3 shows the infrared absorption spectra and X-ray diffraction (XRD) patterns of electro-polymerized EB and LPANI. In Figure 3A, the characteristic PANI absorption peaks at approximately $1,494 \text{ cm}^{-1}$, corresponding to the orthosubstituted quinone-type structure ($\text{N}=\text{Q}=\text{N}$), and $1,582 \text{ cm}^{-1}$, corresponding to the orthosubstituted benzene-type structure of the

aromatic hydrocarbons ($N=B=N$), were observed. The peaks at 1375 cm^{-1} and 1302 cm^{-1} , corresponding to stretching vibrations of aromatic amines ($C=N$) on the PANI skeleton, are typical absorptions for emeraldine salt-type conductive PANI. The peaks at $1,147\text{ cm}^{-1}$, 827 cm^{-1} , and 506 cm^{-1} are corresponding to the C-H in-plane vibration, out-of-plane bending vibration on the benzene ring and the benzene ring bending vibration, respectively. The peak at 793 cm^{-1} represents the 1,4-disubstituted benzene. Compared with the EB absorption peaks, all the absorption peaks of LPANI shifted to the low-frequency region, and the peak width and intensity increased relatively, particularly the two peaks for quinone and benzene. A new absorption peak emerged at approximately 670 cm^{-1} , due to the enhanced delocalization of the conjugated chain by the secondary doping of Li^+ ions. However, as illustrated in Figure 3A(b), the CH_3COOLi dopant did not affect the PANI peak shape, which may be explained by the larger steric hindrance of the CH_3COO^- ions in comparison with Cl^- , making the doping process difficult.

In Figure 3B, a strong diffraction peak appears at 2θ of 20.5° in the XRD spectrum of EB, and a wide diffraction peak emerges in the 2θ range of $23\text{--}29^\circ$, which indicates that EB had a particular crystallinity. After secondary doping, the wide diffraction peaks at 2θ range of $23\text{--}29^\circ$ represent the repeating units on the PANI chain in the horizontal and vertical directions, which may be due to the high orientation of the PANI chain. LPANI formed a stronger crystal orientation, resulting in a higher intensity peak, because the pseudo-protonated doping cations and the charge balance complemented the combination of anions combined with the nitrogen atoms in the PANI molecular chain, producing a structure similar to a quaternary ammonium salt. Deducting the background in Figure 3B, the intensity of the diffraction peaks of LPANI are higher than those of APANI, indicating that the LPANI molecular chain is more ordered and has better crystallization. This result may have occurred because of the different radii of the dopant anions. The redox processes of PANI that accompany doping/de-doping are controlled by the radius of the doping cations or counter anions, which directly determines the doping velocity and doping level. The CH_3COO^- anions suffered larger steric hindrance during the doping/de-doping process because of the larger radius compared to that of Cl^- . Thus, the CH_3COOLi had a lower doping velocity and lower doping level to PANI than LiCl to PANI, which decreased the relative crystallinity of APANI. The relative steric

hindrance of the quinoid-type and benzene-type structures between the PANI molecular chains increased as the CH_3COO^- anion concentration increased, thus, limiting the orderly arrangement of PANI molecular chains and reducing the crystallinity of the product. LPANI with a high doping level opposed more Li^+ cations with free radical charges, which delocalized onto the amine groups on the benzene ring, favoring rearrangement of the PANI molecular chain and blocking the compact arrangement of the chain structure, thereby increasing the conductivity.

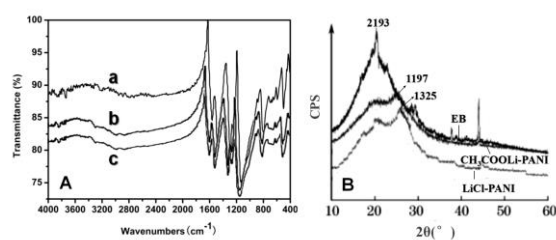


Figure 3: Fourier transform infrared (FT-IR) spectra and X-ray diffraction (XRD) patterns of the electropolymerized EB and secondary doped PANI. A: FT-IR spectra of a, LPANI; b, APANI; c, EB. B: XRD patterns.

CV performance of LPANI was investigated in different electrolyte solutions, as shown in Figure 4. Two pairs of clearly separate redox peaks with relatively symmetrical shape were observed at high peak currents, indicating that PANI doped with Li^+ cations had the best electrochemical redox properties in the present system. The first pair of redox peaks in the potential range of $-0.3\text{--}0.22\text{ V}$ was related to oxidation from leucoemeraldine base (LEB) of PANI to EB and vice versa, accompanied by the doping or off-doping of Li^+ cations, which benefited to the pseudo-protonation of PANI. The second pair of redox peaks in the potential range of $0.6\text{--}0.8\text{ V}$ was related to the reduction from PANI EB to pernigraniline and vice versa, accompanied by the doping or off-doping of anions. Figure 4(b–d) exhibits the typical rectangular shape, suggesting that the present electrolyte system is a promising candidate for the secondary doped PANI cathode. As shown in Figure 4b, $0.3\text{ M CH}_3\text{COOLi}$ doping had a minor impact on the electroactivity of PANI, compared with the doubled peak current at the same LiCl concentration used for the electrolyte, which is consistent with the conclusion drawn from the steric hindrance. Because the radius of Cl^- ions is far smaller than that of CH_3COO^- , the ease of LiCl doping/de-doping induced the higher

electrochemical activity. Initially, the peak current significantly increased with Li^+ concentration. Once the doping concentration was higher than 0.5 M, the Li^+ concentration continued to increase, but the peak current hardly changed, which illustrated that Li^+ doping was saturated in PANI. Therefore, additional LiCl did not improve the electrochemical performance of PANI. Notably, the reduction peak potentials shifted to the left with an increase in LiCl, while the oxidation peak potentials shifted to the right, enlarging the potential difference between the redox peaks. The polarization of the electrode increased with the current, and thus the internal resistance within the circuit increased. However, the potential difference in the two pairs of redox peaks was not over 0.3 V, which illustrated that the electrochemical reactions have excellent reversibility and high Coulomb efficiency.

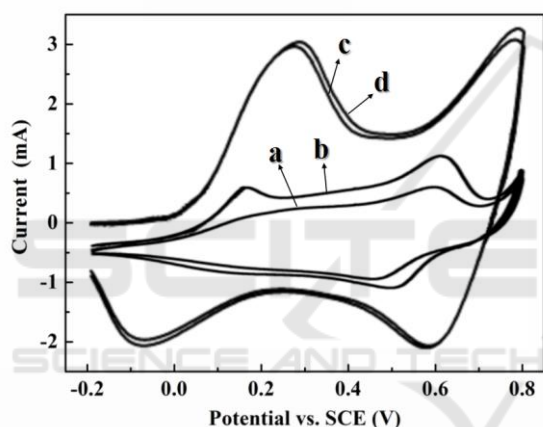


Figure 4: Cyclic voltammetry of LPANI in different electrolyte solutions (pH 4.0): a, PANI in 0.3 M CH_3COOLi solution; b, PANI in 0.3 M LiCl solution; c, PANI in 0.5 M LiCl solution; d, PANI in 0.7 M LiCl solution.

3.3 Discharge Performance of the LPANI Composite Film Cathode Prepared by Coating

The quantities of graphite powder, binder, TiO_2 powder in composite materials and the PANI film thickness in the LPANI composite film cathode were determined by orthogonal tests of four factors at three levels (coded as $L_9(3^4)$) depending on the first discharge capacity (shown in Table 1). Nine groups of LPANI composite film electrodes were prepared, as listed in Table 1, through the steps described in 2.3 and were charged and discharged at a constant current density of $4 \text{ mA}\cdot\text{cm}^{-2}$ in 0.5 M $\text{ZnCl}_2 + 0.5 \text{ M}$

LiCl electrolyte solution, with Zn plates as the anodes for all tested batteries. The voltage upper and lower voltage limits were 1.7 V and 0.7 V, respectively. The first discharge capacity of each electrode was calculated according to the formula for specific capacity (1).

$$F = \frac{t \times J \times A}{m} \tag{1}$$

where F is the discharge capacity ($\text{mAh}\cdot\text{g}^{-1}$), t is the discharge time (h), J is the discharge current density ($\text{mA}\cdot\text{cm}^{-2}$), A is the electrode area (cm^2), and m is the quantity of the PANI film on the electrode (g). The factors affecting the discharge specific capacity of the electrodes were characterized by extreme deviation from the analytical results.

Table 1: The orthogonal tests in $L_9(3^4)$ of LPANI composite film electrodes prepared by coating.

No.	The factors				The first discharge capacity
	A	B	C	D	
1	10	1	0.1	0.1	106.7
2	10	5	0.5	0.2	118.6
3	10	10	1	0.4	103.8
4	20	1	1	0.2	121.9
5	20	5	0.1	0.4	114.2
6	20	10	0.5	0.1	116.8
7	30	1	0.5	0.4	113.3
8	30	5	1	0.1	114.5
9	30	10	0.1	0.2	112.4
$K_1 = \sum y_1$	329.1	341.9	333.3	338	
$K_2 = \sum y_2$	352.9	347.3	348.7	352.9	
$K_3 = \sum y_3$	340.2	333	340.2	331.3	
Range= $K_{\max} - K_{\min}$	23.8	14.3	15.4	21.6	

Note that A, B, C, and D are the wt% of graphite, TiO_2 powder, binder, and the LPANI composite film thickness, respectively. y_{mi} and K_{mi} are the variables and variable sums corresponding to the i -th level of the m -th column factor, respectively. K_{\max} and K_{\min} are the maximum and the minimum variable sums, respectively. R is the range of the m -th column factor.

As shown in Table 1, the magnitude of the range of each parameter is in the order of $A > D > B > C$, which indicates the influence of the factors on the test indexes. The quantity of graphite powder is an important factor affecting the discharge capacity of the composite electrode, as adding graphite powder increased the conductivity of the LPANI composite film electrode, but excess graphite powder resulted

in a lower amount of PANI and a lower electrode discharge capacity. Too thin PANI film led to lower overall electrode discharge capacity lowered; however, a thick film assisted electrode polarization, which resulted in a larger voltage drop. The dosage of TiO₂ powder and crosslinking agent had less of an effect on the discharge capacity than the above factors. Table 1 shows that the optimal conditions for fabricating the LPANI composite film electrodes are 20 wt% graphite powder, 5 wt% TiO₂ powder, and 0.5 wt% binder with a film thickness of 0.2 mm.

3.4 The Charge/Discharge Performance of the Coated Zn Composite//Secondary Doped PANI Composite Film Battery

A charge/discharge performance test of the cell was carried out using the chronopotentialmetry method in 0.5 M ZnCl₂ + 0.5 M LiCl electrolyte solution to evaluate the properties of the assembled coated Zn composite//LPANI composite film battery. The LPANI composite material coated on graphite was used as the cathode, the Zn composite material coated on copper foil was used as the anode, and a SCE was used as the reference electrode. Figure 5A shows the capacity density as the battery voltage was varied between 0.7 V and 1.7 V at different current densities. As the current density increased, the discharge capacity density decreased gradually, and the maximum discharge capacity density reached 131.4 mAh·g⁻¹ at 2 mA·cm⁻², 115.2 mAh·g⁻¹ at 4 mA·cm⁻² and 100.1 mAh·g⁻¹ at 8 mA·cm⁻², due to the following reasons. First, during charge/discharge at constant current, the greater the current density, the higher the overpotential caused by the physical resistance and the irreversible concentration polarization, the much greater the energy loss, and the smaller the capacity is. Because of the overpotential, the actual cut-off voltage for charging was lower than the set value, while the actual cut-off voltage of discharge is higher than the set value, which resulted in a reduced capacity. In addition, the time to form the electric double layer in the micropores, in which the electrolyte had difficulty penetrating, was short at a large current density, and the electrochemical reaction and doping process only occurred on the electrode material surface and did not enter the pores, leading to a low utilization rate of the electrode material and reduced specific capacity. The Coulomb efficiency of the charge/discharge cycle is closely related to the magnitude of the current density. The Coulomb efficiency reached 97% at a current density of 8

mA·cm⁻², while at a current density of 2 mA·cm⁻², the Coulomb efficiency reached 118%, which was ascribed to the oxidation of PANI by ambient oxygen. A battery operated at a lower current density has a longer charge/discharge cycle, in which more PANI is oxidized by oxygen in the atmosphere, and so the Coulomb efficiency increased with a decrease in the current density.

Figure 5B shows the standard charge/discharge curves of the present battery at 4 mA·cm⁻². The charge voltage increased smoothly from the starting voltage of 1.1 V up to 1.7 V, with a steady discharge platform between 1.4 V and 0.8 V. A voltage drop occurred at the beginning of the discharge. Then, the voltage changed smoothly near the end of the discharge. The charge/discharge curve of each cycle was the same, with an average discharge voltage of 1.1 V. The voltage drop at discharge was due to internal resistance and electrode polarization and was proportional to the current density, further confirming our speculation.

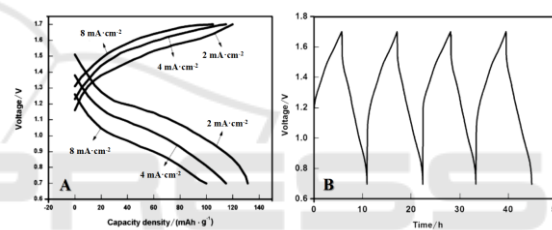


Figure 5: The charge/discharge performance of the coated Zn//secondary doped PANI composites film battery: A, the capacity density response at different current densities; B, the charge/discharge curve at a current density of 4 mA·cm⁻².

Figure 6 shows the relationships of the Coulomb efficiency and discharge capacity to the cycle number of the coated Zn//secondary doped PANI film battery at 4 mA·cm⁻². With an increase in the number of cycles, the discharge capacity density decreased, for example, from 115.2 to 112.4 mAh·g⁻¹ for 35 cycles, with an average discharge capacity density attenuation of 0.07% and with no delamination of active substances from the matrix and almost no change in the Coulomb efficiency, which indicated that the assembled battery had excellent cycle performance and stability. The reduced discharge capacity density contributed to the electrochemical decomposition of the PANI material by peroxidation at a high potential.

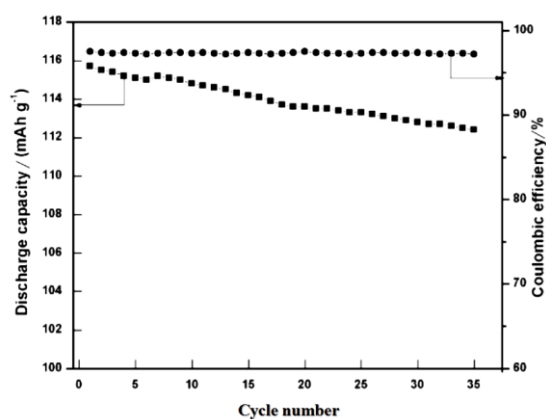


Figure 6: The charge/discharge cycle of the coated Zn/secondary doped PANI composite film battery at a current density of $4 \text{ mA} \cdot \text{cm}^{-2}$.

4 CONCLUSIONS

In conclusion, we have demonstrated the feasibility of rechargeable batteries composed of coated Zn composite//LPANI composite film using LPANI as the main raw conductive materials in the LPTCD cathode and the ZZMCN composite as the anode. The secondary doping of PANI with LiCl after in situ electropolymerization produced a good conductive structure and improved electrochemical activity. The coating preparation method enabled control of the electrode thickness and increased the conductive material capacity on the current collectors. The designed coated Zn composite//LPANI composite film battery showed excellent electrochemical performance and stability, with an average discharge capacity density attenuation of 0.07% and with no delamination of active substances from the matrix during 35 charge/discharge cycles at a current density of $4 \text{ mA} \cdot \text{cm}^{-2}$. Other advantages of the battery included environmental friendliness, low cost, simple production process, and ease of production scale-up. The results suggested that this battery provides a kind potential possible selection for the people to use.

ACKNOWLEDGEMENTS

The authors are grateful to the Nature Science Foundation of China (No.21727810), the Nature Science Foundation of Hunan Province of China

(No.2018JJ5024) and the Nature Science Foundation of Hunan Chemical Vocational Technology College (No.HNHY2017011) for financial support.

CONFLICTS OF INTEREST

Declarations of conflicts of interest: none.

REFERENCE

- Arafa I.M., Ghanem H.M.E., and Bani-Doumi K.A., 2013. *J. Inorg. Organomet. Polym.* 23, pp.365-373.
- Arjomandi J., and Tadayonfar S., 2013. *Polym. composite.*, 35, pp.351-363.
- Bogdanovic U., Vodnik V.V., and Ahrenkiel S.P., 2014. *Synthetic Met.*, 195, pp.122-131.
- Collins J., Kear G., Li X.H., Low C.T.J., Pletcher D., Tangirala, R. D. Stratton-Campbell, Walsh F.C. and Zhang C.P., 2010. *J. Power Sources*, 195, pp.1731-1738.
- Collins J., Li X. H., Pletcher D., R. Tangirala, Stratton-Campbell D., Walsh F. C. and Zhang C. P., 2010. *J. Power Sources*, 195, pp.2975-2978.
- Dinh H.N., Ding J., Xia S.J. and Birss V.I., 1998. *J. Electroanal Chem.*, 459, pp.45-46.
- El-Nowihy G.H., Mohammad A. M., and Khalil M. M. H., *J. Electrochem*, 2017. *Sci.*, 12, pp.40-47.
- El-Nowihy G.H., Mohammad A.M., and Khalil M.M.H., 2017. *J. Electrochem. Sci.* 12, pp.40-48.
- Gao Y., Zhang Y., Yi J., 2016. *Int. Arch. Occ. Env. Hea.*, 89, pp. 1137-1145.
- García-Lugo F., Medel A., and Jurado Baizaval J.L., 2018. *J. Electrochem. Sci.*, 3, pp.196-209.
- Ghanbari K., Mousavi M F., Shamsipur M., 2006. *Electrochi. Acta*, 52 (4), pp.1514-1522.
- Hu J., Jia F, Song Y, 2017. *Chem. Eng. J.*, 326, pp.326-332.
- Hui Y., Cao L., Xu Z., Huang J., Ouyang H., Li J., and Hu H., 2017. *J. Mater. Sci. Technol.*, 33, pp.231-240.
- Hun X., Li Y., Wang S., Li Y., Zhao J., and Luo X., 2018. *Biosens. Bioelectron.*, 112, pp.93-101.
- Kan J., Li X., and Li Y., 2002. *Bull. Electrochem.*, 18, pp.477-480.
- Li S., Zhang G., and Jing G., 2008. *Synth. Met.*, 158, p.242-245.
- Li X.H., Pletcher D. and Walsh F.C., 2009. *Electrochem. Acta*, 54, pp.4688-4695.
- Liang Y. L., Tao Z. L., and Chen J., 2012. *Adv. Energy Mater.*, 2, pp.742-751.
- Liu P., Han J., Jiang L., Li Z., and Cheng J., 2017. *Appl. Surf. Sci.*, 400, pp.446-458.
- Liu S, Zhu K., Zhang Y. and Xu J., 2006. *Polym.*, 47, pp.7680-7688.
- Liu Y., Zhang J., Liu X., Guo J., Pan L., Wang H., Su Q., and Du G., 2014. *Mater. Lett.*, 133, pp.193-202.

- Liu Z., Prowald A., Höfft O., Li G.Z., Lahiri A., and Andres F., 2018. *ChemElectroChem*, 45, pp.67-76.
- Mini V., Kamath A., Raghu S., Sharanappa C., and Devendrappa H., 2014. *Ind. Eng. Chem. Res.*, 53, pp.16873-16881.
- Mirmohseni A., and Solhjo R., 2003. *Eur. Polym. J.*, 39, pp.219-223.
- Nishio K., and Furukawa N., 2007. *Handbook of Battery Materials*, 1st edition, Hoboken: Wiley Press, pp.43-87.
- Pandey K., Asthana N., Sanjay S.S., and Dwivedi M.M., 2016. *Eur. J. Adv. Eng. Technol.*, 3, pp.21-29.
- Paral M.M.P., Gillado A.V., and Herrera M.U., 2018. *Surf. Inter.*, 10, pp.74-78.
- Pirkarami A., Olya M.E., and Limaee N.Y., 2013. *Prog. Org. Coat.*, 76, pp.682-674.
- Pletcher D., Zhou H., Kear G., Low C.T.J., Walsh F.C. and Wills R.G.A., 2008. *J. Power Sources*, 180, pp.621-629.
- Pletcher D., Zhou H., Kear G., Low C.T.J., Walsh F.C. and Wills R.G.A., 2008. *J. Power Sources*, 180, pp.630-634.
- Pourabdollah, Kobra, 2017. *Chem. Eng. Sci.*, 160, pp.304-312.
- Pozo- Gonzalo C., 2015. *ChemElectroChem*, 2, pp.2071-2080.
- Ramirez F.C.R., Ramakrishnan P., Flores-Payag Z.P., Shanmugam S., and Binag C., 2017. *Synthetic Met.*, 230, pp.65-74.
- Rana U., Paul N. D., Mondal S., Chakraborty C., and Malik S., 2014. *Synthetic Met.*, 192, pp.43-50.
- Sevil U.A., Coskun E., and Günen O., 2014. *Rad. Phys. Chem.*, 94, pp.45-54.
- Silva M.J.D., Sanches A.O., Malmonge L.F., and Malmonge J.A., 2014. *Mater. Res.*, 17, pp.59-68.
- Sivaraman P., Thakur A.P., and Kushwaha R.K., 2008. *J. Appl. Electrochem.*, 38, p.189-195.
- Skotheim T.M., Elsenbaumer R.L., and Reynolds J.R., 1997. *Handbook of Conducting Polymers*. 1st edition. New York: CRC Press, pp.11-38.
- Taheri N. N., Ramezandeh B., Mahdavian M., and Bahlakeh G., 2018. *J. Ind. Eng. Chem.*, 63, pp.322-331.
- Tran C., Singhal R., Lawrence D., and Kalra V., 2015. *J. Power Sources*, 293, pp.373-379.
- Vatsalarani J., Trivedi D.C., and Ragavendran K., 2005. *J. Electrochem. Soc.*, 152, pp.1974-1978.
- Wang H., Liu Z., and Li H.Y., 2018. *J. Electrochem. Sci.*, 13, pp.136-148.
- Wang Y.M., 2018. *Polym. Int.*, 67, pp.650-662.
- Wilken S., Johansson P., and Jacobsson P., 2013. *Lithium Batteries*, 1st edition, Hoboken: Wiley Press, pp.146-171.
- Wills R.G.A., Collins J., Stratton-Campbell D., Low C. T. J., Pletcher D. and Walsh F. C., 2010. *J. Appl. Electrochem.*, 40, pp.955-965.
- Xu H., Tang J., Chen Y., Liu J., Pu J., and Li Q., 2017. *J. Electron. Mater.*, 46, pp.6150-6158.
- Xu H., Zhang J.L., Chen Y., Lu H.L., and Zhuang J.X., 2014. *RSC Adv.* 4, pp. 9-21.
- Yazvinskaya, Nataliya N, Galushkin, and Nikolay E, 2017. *Int. J. Electrochem., Sci*, 12, pp.2791-2797.
- Yesappa L., Niranjana M., Ashokkumar S.P., Vijeth H., Sharanappa C., Raghu S., and Devendrappa H., 2017. *J. Electron. Mater.*, 46, pp.6965-6973.
- Yi L., Liu L., Guo G., Chen X., Zhang Y., Yu S., and Wang X., 2017. *Electrochim. Acta*, 240, pp.63-71.
- Yoshitaka I., Shinichi S., Tadashi T., 2017. *Electr. Eng. Jpn.*, 201, pp.14-24.
- Zhang H., Qin G., Lin Y., Zhang D., Liao H., Li Z., Tian J., and Wu Q., 2018. *Electrochim. Acta*, 264, pp.91-98.
- Zhang X., Wang Y., Li Y., 2015. *J. Inorg. Mater.*, 30, pp.739-744.
- Zhao Z., Yu T., Miao Y., and Zhao X., 2018. *Electrochim. Acta*, 270, pp.30-38.